
Evolving Normalization-Activation Layers

Hanxiao Liu[†], Andrew Brock[‡], Karen Simonyan[‡], Quoc V. Le[†]

[†]Google Research, Brain Team [‡]DeepMind
{hanxiao1, ajbrock, simonyan, qvl}@google.com

Abstract

Normalization layers and activation functions are fundamental components in deep networks and typically co-locate with each other. Here we propose to design them using an automated approach. Instead of designing them separately, we unify them into a single tensor-to-tensor computation graph, and evolve its structure starting from basic mathematical functions. Examples of such mathematical functions are addition, multiplication and statistical moments. The use of low-level mathematical functions, in contrast to the use of high-level modules in mainstream NAS, leads to a highly sparse and large search space which can be challenging for search methods. To address the challenge, we develop efficient rejection protocols to quickly filter out candidate layers that do not work well. We also use multi-objective evolution to optimize each layer’s performance across many architectures to prevent overfitting. Our method leads to the discovery of *EvoNorms*, a set of new normalization-activation layers with novel, and sometimes surprising structures that go beyond existing design patterns. For example, some *EvoNorms* do not assume that normalization and activation functions must be applied sequentially, nor need to center the feature maps, nor require explicit activation functions. Our experiments show that *EvoNorms* work well on image classification models including ResNets, MobileNets and EfficientNets but also transfer well to Mask R-CNN with FPN/SpineNet for instance segmentation and to BigGAN for image synthesis, outperforming BatchNorm and GroupNorm based layers in many cases.¹

1 Introduction

Normalization layers and activation functions are fundamental building blocks in deep networks for stable optimization and improved generalization. Although they frequently co-locate, they are designed separately in previous works. There are several heuristics widely adopted during the design process of these building blocks. For example, a common heuristic for normalization layers is to use mean subtraction and variance division [1–4], while a common heuristic for activation functions is to use scalar-to-scalar transformations [5–11]. These heuristics may not be optimal as they treat normalization layers and activation functions as separate. Can automated machine learning discover a novel building block to replace these layers and go beyond the existing heuristics?

Here we revisit the design of normalization layers and activation functions using an automated approach. Instead of designing them separately, we unify them into a normalization-activation layer. With this unification, we can formulate the layer as a tensor-to-tensor computation graph consisting of basic mathematical functions such as addition, multiplication and cross-dimensional statistical moments. These low-level mathematical functions form a highly sparse and large search space, in contrast to mainstream NAS which uses high-level modules (e.g., Conv-BN-ReLU). To address the challenge of the size and sparsity of the search space, we develop novel rejection protocols to efficiently filter out candidate layers that do not work well. To promote strong generalization across different architectures, we use multi-objective evolution to explicitly optimize each layer’s

¹Code for *EvoNorms* on ResNets: <https://github.com/tensorflow/tpu/tree/master/models/official/resnet>

BN-ReLU	$\max\left(\frac{x - \mu_{b,w,h}(x)}{\sqrt{s_{b,w,h}^2(x)}} \gamma + \beta, 0\right)$
EvoNorm-B0	$\frac{x}{\max(\sqrt{s_{b,w,h}^2(x)}, v_1 x + \sqrt{s_{w,h}^2(x)})} \gamma + \beta$

Table 1: A searched layer named EvoNorm-B0 which consistently outperforms BN-ReLU. $\mu_{b,w,h}$, $s_{b,w,h}^2$, $s_{w,h}^2$, v_1 refer to batch mean, batch variance, instance variance and a learnable variable.

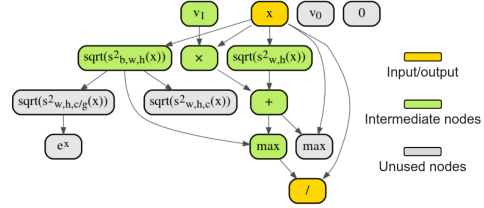


Figure 1: Computation graph of EvoNorm-B0.

performance over multiple architectures. Our method leads to the discovery of a set of novel layers, dubbed EvoNorms, with surprising structures that go beyond expert designs (an example layer is shown in Table 1 and Figure 1). For example, our most performant layers allow normalization and activation functions to interleave, in contrast to BatchNorm-ReLU or ReLU-BatchNorm [1, 12] where normalization and activation function are applied sequentially. Some EvoNorms do not attempt to center the feature maps, and others require no explicit activation functions.

EvoNorms consist of two series: B series and S series. The B series are batch-dependent and were discovered by our method without any constraint. The S series work on individual samples, and were discovered by rejecting any batch-dependent operations. We verify their performance on a number of image classification architectures, including ResNets [13], MobileNetV2 [14] and EfficientNets [15]. We also study their interactions with a range of data augmentations, learning rate schedules and batch sizes, from 32 to 1024 on ResNets. Our experiments show that EvoNorms can substantially outperform popular layers such as BatchNorm-ReLU and GroupNorm-ReLU. On Mask R-CNN [16] with FPN [17] and with SpineNet [18], EvoNorms achieve consistent gains on COCO instance segmentation with negligible computation overhead. To further verify their generalization, we pair EvoNorms with a BigGAN model [19] and achieve promising results on image synthesis.

Our contributions can be summarized as follows:

- We are the first to search for the combination of normalization-activation layers. Our proposal to unify them into a single graph and the search space are novel. Our work tackles a missing link in AutoML by providing evidence that it is possible to use AutoML to discover a new building block from low-level mathematical operations (see Sec. 2 for a comparison with related works). A combination of our work with traditional NAS may realize the full potential of AutoML in automatically designing machine learning models from scratch.
- We propose novel rejection protocols to filter out candidates that do not work well or fail to work, based on both their performance and stability. We are also the first to address strong generalization of layers by pairing each candidate with multiple architectures and to explicitly optimize their cross-architecture performance. Our techniques can be used by other AutoML methods that have large, sparse search spaces and require strong generalization.
- Our discovered layers, EvoNorms, by themselves are novel contributions because they are different from previous works. They work well on a diverse set of architectures, including ResNets [12, 13], MobileNetV2 [14], MnasNet [20], EfficientNets [15], and transfer well to Mask R-CNN [16], SpineNet [21] and BigGAN-deep [19]. E.g., on Mask-RCNN our gains are +1.9AP over BN-ReLU and +1.3AP over GN-ReLU. EvoNorms have a high potential impact because normalization and activation functions are central to deep learning.
- EvoNorms shed light on the design of normalization and activation layers. E.g., their structures suggest the potential benefits of non-centered normalization schemes, mixed variances and tensor-to-tensor rather than scalar-to-scalar activation functions (these properties can be seen in Table 1). Some of these insights can be used by experts to design better layers.

2 Related Works

Separate efforts have been devoted to design better activation functions and normalization layers, either manually [1–4, 7–10, 22] or automatically [11, 23]. Different from the previous works, we eliminate the boundary between normalization and activation layers and search them jointly as a unified building block. Our search space is more challenging than those in the existing automated approaches [11, 23]. For example, we avoid relying on common heuristics like mean subtraction

or variance division in handcrafted normalization schemes; we search for general tensor-to-tensor transformations instead of scalar-to-scalar transformations in activation function search [11].

Our approach is inspired by recent works on neural architecture search, e.g., [20, 24–49], but has a very different goal. While existing works aim to specialize an architecture built upon well-defined building blocks such as Conv-BN-ReLU or inverted bottlenecks [14], we aim to discover new building blocks starting from low-level mathematical functions. Our motivation is similar to AutoML-Zero [50] but has a more practical focus: the method not only leads to novel building blocks with new insights, but also achieves competitive results across many large-scale computer vision tasks.

Our work is also related to recent efforts on improving the initialization conditions for deep networks [51–53] in terms of challenging the necessity of traditional normalization layers. While those techniques are usually architecture-specific, our method discovers layers that generalize well across a variety of architectures and tasks without specialized initialization strategies.

3 Search Space

Layer Representation. We represent each normalization-activation layer as a computation graph that transforms an input tensor into an output tensor (an example is shown in Figure 1). The computation graph is a DAG that has 4 initial nodes, including the input tensor and three auxiliary nodes: a constant zero tensor, and two trainable vectors v_0 and v_1 along the channel dimension initialized as 0’s and 1’s, respectively. In general, the DAG can have any number of nodes, but we restrict the total number of nodes to $4+10=14$ in our experiments. Each intermediate node in the DAG represents the outcome of either a unary or a binary operation (shown in Table 2).

Primitive Operations. Table 2 shows the primitive operations in the search space, including element-wise operations and aggregation operations that enable communication across different axes of the tensor.

Here we explain the notations \mathcal{I} , μ , and s in the Table for aggregation ops. First, an aggregation op needs to know the axes (index set) where it can operate, which is denoted by \mathcal{I} . Let x be a 4-dimensional tensor of feature maps. We use b, w, h, c to refer to its batch, width, height and channel dimensions, respectively. We use $x_{\mathcal{I}}$ to represent a subset of x ’s elements along the dimensions indicated by \mathcal{I} . For example, $\mathcal{I} = (b, w, h)$ indexes all the elements of x along the batch, width and height dimensions; $\mathcal{I} = (w, h)$ refers to elements along the spatial dimensions only.

The notations μ and s indicate ops that compute statistical moments, a natural way to aggregate over a set of elements. Let $\mu_{\mathcal{I}}(x)$ be a mapping that replaces each element in x with the 1st order moment of $x_{\mathcal{I}}$. Likewise, let $s_{\mathcal{I}}^2(x)$ be a mapping that transforms each element of x into the 2nd order moment among the elements in $x_{\mathcal{I}}$. Note both $\mu_{\mathcal{I}}$ and $s_{\mathcal{I}}^2$ preserve the shape of the original tensor.

Finally, we use \cdot/g to indicate that aggregation is carried out in a grouped manner along a dimension. We allow \mathcal{I} to take values among (b, w, h) , (w, h, c) , (w, h) and $(w, h, c/g)$. Combinations like $(b, w/g, h, c)$ or $(b, w, h/g, c)$ are not considered to ensure the model remains fully convolutional.

Random Graph Generation. A random computation graph in our search space can be generated in a sequential manner. Starting from the initial nodes, we generate each new node by randomly sampling a primitive op and then randomly sampling its input nodes according to the op’s arity. The process is repeated multiple times and the last node is used as the output.

With the above search space, we perform several small scale experiments with random sampling to understand its behaviors. Our observations are as follows:

Element-wise Ops	Expression	Arity
Add	$x + y$	2
Mul	$x \times y$	2
Div	x/y	2
Max	$\max(x, y)$	2
Neg	$-x$	1
Sigmoid	$\sigma(x)$	1
Tanh	$\tanh(x)$	1
Exp	e^x	1
Log	$\text{sign}(x) \cdot \ln(x)$	1
Abs	$ x $	1
Square	x^2	1
Sqrt	$\text{sign}(x) \cdot \sqrt{ x }$	1
Aggregation Ops	Expression	Arity
1 st order	$\mu_{\mathcal{I}}(x)$	1
2 nd order	$\sqrt{\mu_{\mathcal{I}}(x^2)}$	1
2 nd order, centered	$\sqrt{s_{\mathcal{I}}^2(x)}$	1

Table 2: Search space primitives. The index set \mathcal{I} can take any value among $\{(b, w, h), (w, h, c), (w, h), (w, h, c/g)\}$. A small ϵ is inserted as necessary for numerical stability. All the operations preserve the shape of the input tensor.

Observation 1: High sparsity of the search space. While our search space can be expanded further, it is already large enough to be challenging. As an exercise, we took 5000 random samples from the search space and plugged them into three architectures on CIFAR-10. Figure 2 shows that none of the 5000 samples can outperform BN-ReLU. The accuracies for the vast majority of them are no better than random guess (note the y-axis is in log scale). A typical random layer would look like $\text{sign}(z)\sqrt{z\gamma} + \beta$, $z = \sqrt{s_{w,h}^2(\sigma(|x|))}$ and leads to near-zero ImageNet accuracies. Although random search does not seem to work well, we will demonstrate later that with a better search method, this search space is interesting enough to yield performant layers with highly novel structures.

Observation 2: Weak generalization across architectures. It is our goal to develop layers that work well across many architectures, e.g., ResNets, MobileNets, EfficientNets etc. We refer to this as *strong generalization* because it is a desired property of BatchNorm-ReLU. As another exercises, we pair each of the 5000 samples with three different architectures, and plot the accuracy calibrations on CIFAR-10. The results are shown in Figure 3, which indicate that layers that perform well on one architecture can fail completely on the other ones. Specifically, a layer that performs well on ResNets may not enable meaningful learning on MobileNets or EfficientNets at all.

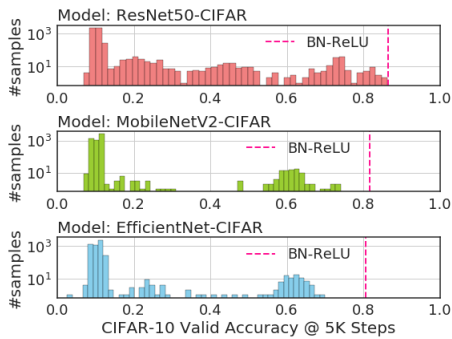


Figure 2: CIFAR-10 accuracy histograms of 5K random layers over three architectures.

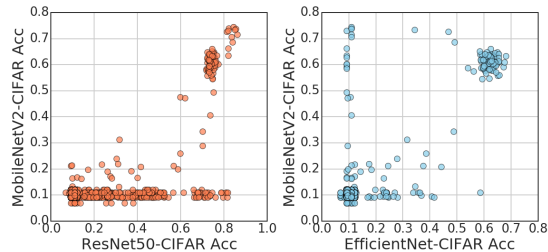


Figure 3: CIFAR-10 accuracy calibrations of 5K random layers over three architectures. The calibration is far from perfect. For example, layers performing well on ResNet-CIFAR may not be able to outperform random guess on MobileNetV2-CIFAR.

4 Search Method

In this section, we propose to use evolution as the search method (Sec. 4.1), and modify it to address the sparsity and achieve strong generalization. In particular, to address the sparsity of the search space, we propose efficient rejection protocols to filter out a large number of undesirable layers based on their quality and stability (Sec. 4.2). To achieve strong generalization, we propose to evaluate each layer over many different architectures and use multi-objective optimization to explicitly optimize its cross-architecture performance (Sec. 4.3).

4.1 Evolution

Here we propose to use evolution to search for better layers. The implementation is based on a variant of tournament selection [54]. At each step, a tournament is formed based on a random subset of the population. The winner of the tournament is allowed to produce offspring, which will be evaluated and added into the population. The overall quality of the population hence improves as the process repeats. We also regularize the evolution by maintaining a sliding window of only the most recent portion of the population [40]. To produce an offspring, we mutate the computation graph of the winning layer in three steps. First, we select an intermediate node uniformly at random. Then we replace its current operation with a new one in Table 2 uniformly at random. Finally, we select new predecessors for this node among existing nodes in the graph uniformly at random.

4.2 Rejection protocols to address high sparsity of the search space

Although evolution improves sample efficiency over random search, it does not resolve the high sparsity issue of the search space. This motivates us to develop two rejection protocols to filter out bad layers after short training. A layer must pass both tests to be considered by evolution.

Quality. We discard layers that achieve less than 20%² CIFAR-10 validation accuracy after training for 100 steps. Since the vast majority of the candidate layers attain poor accuracies, this simple mechanism ensures the compute resources to concentrate on the full training of a small number of promising candidates. Empirically, this speeds up the search by up to two orders of magnitude.

Stability. In addition to quality, we reject layers that are subject to numerical instability. The basic idea is to stress-test the candidate layer by *adversarially* adjusting the model weights θ towards the direction of maximizing the network’s gradient norm. Formally, let $\ell(\theta, G)$ be the training loss of a model when paired with computation graph G computed based on a small batch of images. Instability of training is reflected by the worst-case gradient norm: $\max_{\theta} \|\partial\ell(\theta, G)/\partial\theta\|_2$. We seek to maximize this value by performing gradient ascent along the direction of $\frac{\partial\|\partial\ell(\theta, G)/\partial\theta\|_2}{\partial\theta}$ up to 100 steps. Layers whose gradient norm exceeding 10^8 are rejected. The stability test focuses on robustness because it considers the worst case, hence is complementary to the quality test. This test is highly efficient—gradients of many layers are forced to quickly blow up in less than 5 steps.

4.3 Multi-architecture evaluation to promote strong generalization

To explicitly promote strong generalization, we formulate the search as a multi-objective optimization problem, where each candidate layer is always evaluated over multiple different *anchor* architectures to obtain a set of fitness scores. We choose three architectures as the anchors, including ResNet50 [13] (v2)³, MobileNetV2 [14] and EfficientNet-B0 [15]. Widths and strides of these Imagenet architectures are adapted w.r.t the CIFAR-10 dataset [55] (Appendix B), on which they will be trained and evaluated for speedy feedback. The block definitions of the anchor architectures are shown in Figure 4.

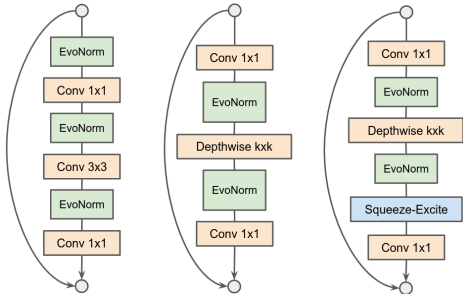


Figure 4: Block definitions of anchor architectures: ResNet-CIFAR (*left*), MobileNetV2-CIFAR (*center*), and EfficientNet-CIFAR (*right*).⁴

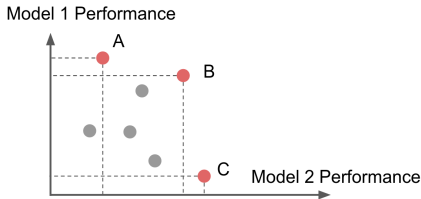


Figure 5: Illustration of tournament selection criteria for multi-objective optimization. Candidate B wins under the Average criterion. Each of A, B, C wins with probability $\frac{1}{3}$ under the Pareto criterion.

Tournament Selection Criterion. As each layer is paired with multiple architectures, and therefore has multiple scores, there are multiple ways to decide the tournament winner within evolution:

Average: Layer with the highest average accuracy wins (e.g., B in Figure 5 wins because it has the highest average performance on the two models.).

Pareto: A random layer on the Pareto frontier wins (e.g., A, B, C in Figure 5 are equal likely to win as none of them can be dominated by other candidates.).

Empirically we observe that different architectures have different accuracy variations. For example, ResNet has been observed to have a higher accuracy variance than MobileNet and EfficientNet on CIFAR-10 proxy tasks. Hence, under the Average criterion, the search will bias towards helping ResNet, not MobileNet nor EfficientNet. We therefore propose to use the Pareto frontier criterion to avoid this bias. Our method is novel, but reminiscent of NSGA-II [56], a well-established multi-objective genetic algorithm, in terms of simultaneously optimizing all the non-dominated solutions.

²This is twice as good as random guess on CIFAR-10.

³We always use the v2 instantiation of ResNets [13] where ReLUs are adjacent to BatchNorm layers.

⁴For each model, a custom layer is used to replace BN-ReLU/Swish in the original architecture. Each custom layer is followed by a channel-wise affine transform. See pseudocode in Appendix A for details.

5 Experiments

We include details of our experiments in Appendix C, including settings and hyperparameters of the proxy task, search method, reranking, and full-fledged evaluations. In summary, we did the search on CIFAR-10, and re-ranked the top-10 layers on a held-out set of ImageNet to obtain the best 3 layers. The top-10 layers are reported in Appendix D. For all results below, our layers and baseline layers are compared under identical training setup. Hyperparameters are directly inherited from the original implementations (usually in favor of BN-based layers) without tuning w.r.t EvoNorms.

5.1 Generalization across Image Classifiers

Batch-dependent Layers. In Table 3, we compare the three discovered layers against some widely used normalization-activation layers on ImageNet, including strong baselines with the searched Swish activation function [11]. We refer to our layers as the EvoNorm-B series, as they involve **B**atch aggregations ($\mu_{b,w,h}$ and $s_{b,w,h}^2$) hence require maintaining a moving average statistics for inference. The table shows that EvoNorms are no worse than BN-ReLU across all cases, and perform better on average than the strongest baseline. It is worth emphasizing that hyperparameters and architectures used in the table are implicitly optimized for BatchNorms due to historical reasons.

Layer	Expression	R-50				MV2	MN	EN-B0	EN-B5
		original	+aug	+aug+2×	+aug+2×+cos				
BN-ReLU	$\max(z, 0), \frac{x - \mu_{b,w,h}(x)}{\sqrt{s_{b,w,h}^2(x)}}\gamma + \beta$	76.3±0.1	76.2±0.1	77.6±0.1	77.7±0.1	73.4±0.1	74.6±0.2	76.4	83.6
BN-Swish	$z\sigma(v_1z), z = \frac{x - \mu_{b,w,h}(x)}{\sqrt{s_{b,w,h}^2(x)}}\gamma + \beta$	76.6 ±0.1	77.3±0.1	78.2 ±0.1	78.2±0.0	74.5±0.1	75.3 ±0.1	77.0	83.5
Random	$\text{sign}(z)\sqrt{z}\gamma + \beta, z = \sqrt{s_{w,h}^2(\sigma(x))}$	1e-3	1e-3	1e-3	1e-3	1e-3	1e-3	1e-3	1e-3
Random + rej	$\tanh(\max(x, \tanh(x)))\gamma + \beta$	71.7±0.2	70.8±0.1	63.6±18.9	55.3±17.5	1e-3	1e-3	1e-3	1e-3
RS + rej	$\frac{\max(x, 0)}{\sqrt{\mu_{b,w,h}(x^2)}}\gamma + \beta$	75.8±0.1	76.3±0.0	77.4±0.1	77.5±0.1	73.5±0.1	74.6±0.1	76.4	83.2
EvoNorm-B0	$\frac{x}{\max(\sqrt{s_{b,w,h}^2(x)}, v_1x + \sqrt{s_{w,h}^2(x)})}\gamma + \beta$	76.6 ±0.0	77.7 ±0.1	77.9±0.1	78.4 ±0.1	75.0 ±0.1	75.3 ±0.0	76.8	83.6
EvoNorm-B1	$\frac{x}{\max(\sqrt{s_{b,w,h}^2(x)}, (x+1)\sqrt{\mu_{w,h}(x^2)})}\gamma + \beta$	76.1±0.1	77.5±0.0	77.7±0.0	78.0±0.1	74.6±0.1	75.1±0.1	76.5	83.6
EvoNorm-B2	$\frac{x}{\max(\sqrt{s_{b,w,h}^2(x)}, \sqrt{\mu_{w,h}(x^2)} - x)}\gamma + \beta$	76.6 ±0.2	77.7 ±0.1	78.0±0.1	78.4 ±0.1	74.6±0.1	75.0±0.1	76.6	83.4

Table 3: ImageNet results of batch-dependent normalization-activation layers. Terms requiring moving average statistics are highlighted in blue. Each layer is evaluated on ResNets (R), MobileNetV2 (MV2), MnasNet-B1 (MN) and EfficientNets (EN). We also vary the training settings for ResNet-50: “aug”, “2×” and “cos” refer to the use of RandAugment [57], longer training (180 epochs instead of 90) and cosine learning rate schedule [58], respectively. Results in the same column are obtained using identical training setup. Entries with error bars are aggregated over three independent runs.

Table 3 also shows that a random layer in our search space only achieves near-zero accuracy on ImageNet. It then shows that with our proposed rejection rules in Sec. 4.2 (Random + rej), one can find a layer with meaningful accuracies on ResNets. Finally, using comparable compute with evolution, random search with rejection (RS + rej) can discover a compact variant of BN-ReLU. This layer achieves promising results across all architectures, albeit clearly worse than EvoNorms. The search progress of random search relative to evolution is shown in Figure 6 and in Appendix E.

Batch-independent Layers. Table 4 presents EvoNorms obtained from another search experiment, during which layers containing batch aggregation ops are excluded. The goal is to design layers that rely on individual samples only, a desirable property to simplify implementation and to stabilize training with small batch sizes. We refer to these Sample-based layers as the EvoNorm-S series. We compare them against handcrafted baselines designed under a similar motivation, including Group Normalization [4] (GN-ReLU) and a recently proposed layer aiming to eliminate batch dependencies [22] (FRN). Table 4 and its accompanying figure show that EvoNorm-S layers achieve competitive or better results than all the baselines across a wide range of batch sizes.

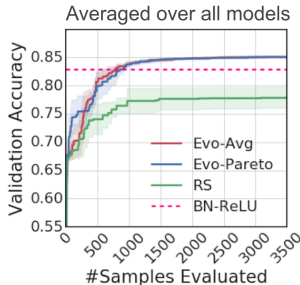


Figure 6: Search progress on CIFAR-10. Each curve is averaged over the top-10 layers in the population and over the three anchor architectures. Only samples survived the quality and stability tests are considered.

Layer	Expression	ResNet-50				MobileNetV2	
		original		+aug+2×+cos		large 128 × 32	small 4 × 32
		large 128 × 8	small 4 × 8	large 128 × 8	small 4 × 8		
BN-ReLU	$\max(z, 0), z = \frac{x - \mu_{w,h}(x)}{\sqrt{s_{w,h}^2(x)}} \gamma + \beta$	76.3±0.1	70.9±0.3	77.7±0.1	70.5±1.1	73.4±0.1	66.7±1.9
GN-ReLU	$\max(z, 0), z = \frac{x - \mu_{w,h,c/g}(x)}{\sqrt{s_{w,h,c/g}^2(x)}} \gamma + \beta$	75.3±0.1	75.8±0.1	77.1±0.1	77.2±0.1	72.2±0.1	72.4±0.1
FRN	$\max(z, v_0), z = \frac{x}{\sqrt{\mu_{w,h}(x^2)}} \gamma + \beta$	75.6±0.1	75.9±0.1	54.7±14.3	77.4±0.1	73.4±0.2	73.5±0.1
EvoNorm-S0	$\frac{x\sigma(v_1x)}{\sqrt{s_{w,h,c/g}^2(x)}} \gamma + \beta$	76.1±0.1	76.5 ±0.1	78.3 ±0.1	78.3 ±0.1	73.9 ±0.2	74.0 ±0.1
EvoNorm-S1	$\frac{x\sigma(x)}{\sqrt{s_{w,h,c/g}^2(x)}} \gamma + \beta$	76.1±0.1	76.3±0.1	78.2±0.1	78.2±0.1	73.6±0.1	73.7±0.1
EvoNorm-S2	$\frac{x\sigma(x)}{\sqrt{\mu_{w,h,c/g}(x^2)}} \gamma + \beta$	76.0±0.1	76.3±0.1	77.9±0.1	78.0±0.1	73.7±0.1	73.8±0.1

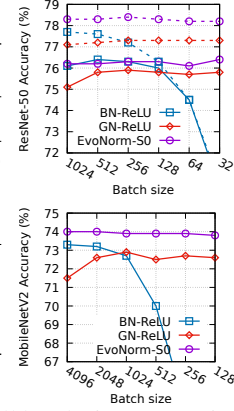


Table 4: *Left*: ImageNet results of batch-independent layers with large and small batch sizes. Learning rates are scaled linearly relative to the batch sizes [59]. For ResNet-50 we report results under both the standard training setting and the fancy setting (+aug+2×+cos). We also report full results under four different training settings in Appendix E. *Right*: Performance as the batch size decreases. For ResNet, solid and dashed lines are obtained with standard setting and fancy setting, respectively.

5.2 Generalization to Instance Segmentation

To investigate if our discovered layers generalize beyond the classification task that we searched on, we pair them with Mask R-CNN [16] for object detection and instance segmentation on COCO [60]. We consider two different types of backbones: ResNet-FPN [17] and SpineNet [21]. The latter is particularly interesting because the architecture has a highly non-linear layout which is very different from the classification models used during search. In all of our experiments, EvoNorms are applied to both the backbone and the heads to replace their original activation-normalization layers. Detailed training settings of these experiments are available in Appendix C.

Backbone	Layer	AP ^{bbox}	AP ^{bbox} ₅₀	AP ^{bbox} ₇₅	AP ^{mask}	AP ^{mask} ₅₀	AP ^{mask} ₇₅	MAdds (B)	Params (M)	Batch Indep.
R-50-FPN	BN-ReLU	42.1	62.9	46.2	37.8	60.0	40.6	379.7	46.37	
	BN-Swish	(+1.0)43.1	63.8	47.3	(+0.6)38.4	60.6	41.4	379.9	46.38	✗
	EvoNorm-B0	(+1.9) 44.0	65.2	48.1	(+1.7) 39.5	62.7	42.4	380.4	46.38	
	EvoNorm-S0	(+0.9) 43.6	64.9	47.9	(+1.0) 39.4	62.3	42.7	380.4	46.38	✓
SpineNet-96	BN-ReLU	47.1	68.0	51.5	41.5	65.0	44.3	315.0	55.19	
	BN-Swish	(+0.5)47.6	68.2	52.0	(+0.5)42.0	65.6	45.5	315.2	55.21	✗
	EvoNorm-B0	(+0.9) 48.0	68.7	52.6	(+0.9) 42.4	66.2	45.8	315.8	55.21	
	EvoNorm-S0	(+1.8) 47.5	68.5	51.8	(+1.1) 42.1	65.9	45.3	315.8	55.21	✓

Table 5: Mask R-CNN object detection and instance segmentation results on COCO val2017.

Results are summarized in Table 5. With both ResNet-FPN and SpineNet backbones, EvoNorms significantly improve the APs with negligible impact on FLOPs or model sizes. While EvoNorm-B0 offers the strongest results, EvoNorm-S0 outperforms commonly used layers, including GN-ReLU and BN-ReLU, by a clear margin without requiring moving-average statistics. These results demonstrate strong generalization beyond the classification task that the layers were searched on.

5.3 Generalization to GAN Training

We further test the applicability of EvoNorms to training GANs [61]. Normalization is particularly important because the unstable dynamics of the adversarial game render training sensitive to nearly every aspect of its setup. We replace the BN-ReLU layers in the generator of BigGAN-deep [19] with EvoNorms and with previously designed layers, and measure performance on ImageNet generation at 128×128

Layer	IS (median/best)	FID (median/best)
BN-ReLU	118.77/124.01	7.85/7.29
EvoNorm-B0	101.13/113.63	6.91/5.87
GN-ReLU	99.09	8.14
LayerNorm-ReLU	91.56	8.35
PixelNorm-ReLU	88.58	10.41
EvoNorm-S0	104.64/113.96	6.86/6.26

Table 6: BigGAN-deep results w. batch-dependent and batch-independent layers. We report median and best performance across 3 random seeds.

resolution using Inception Score (IS, [62]) and Fréchet Inception distance (FID, [63]). We compare two of our most performant layers, B0 and S0, against the baseline BN-ReLU and GN-ReLU, as well as LayerNorm-ReLU [2], and PixelNorm-ReLU [64], a layer designed for a different GAN architecture. We sweep the number of groups in GN-ReLU from 8,16,32, and report results using 16 groups. Consistent with BigGAN training, we report results at peak performance in Table 6. Note higher is better for IS, lower is better for FID.

Swapping BN-ReLU out for most other layers substantially cripples training, but both EvoNorm-B0 and S0 achieve comparable, albeit worse IS, and improved FIDs over the BN-ReLU baseline. Notably, EvoNorm-S0 outperforms all the other per-sample normalization-activation layers in both IS and FID. This result further confirms that EvoNorms transfer to visual tasks in multiple domains.

5.4 Intriguing Properties of EvoNorms

EvoNorm-B0. Unlike conventional normalization schemes relying on a single type of variance only, EvoNorm-B0 mixes together two types of statistical moments in its denominator, namely $s_{b,w,h}^2(x)$ (batch variance) and $s_{w,h}^2(x)$ (instance variance). The former captures global information across images in the same mini-batch, and the latter captures local information per image. It is also interesting to see that B0 does not have any explicit activation function because of its intrinsically nonlinear normalization process. Table 7 shows that manual modifications to the structure of B0 can substantially cripple the training, demonstrating its local optimality.

Expression	Modification	Accuracy (%)		
$\frac{x}{\max(\sqrt{s_{b,w,h}^2(x)}, v_1x + \sqrt{s_{w,h}^2(x)})}$	None	76.5	76.6	76.6
$\frac{x}{\max(\sqrt{s_{b,w,h}^2(x)}, \sqrt{s_{w,h}^2(x)})}$	No v_1x	14.4	50.5	22.0
$\frac{x}{\sqrt{s_{b,w,h}^2(x)}}$	No local term	4.2	4.1	4.1
$\frac{v_1x + \sqrt{s_{w,h}^2(x)}}{x}$	No global term	1e-3	1e-3	1e-3
$\frac{x}{\sqrt{s_{b,w,h}^2(x) + v_1x + \sqrt{s_{w,h}^2(x)}}}$	max \rightarrow add	1e-3	1e-3	1e-3

Table 7: Impact of structural changes to EvoNorm-B0. For each variant we report its ResNet-50 ImageNet accuracies over three random seeds at the point when NaN error (if any) occurs.

EvoNorm-S0. It is interesting to observe the Swish activation function [11] as a part of EvoNorm-S0. The algorithm also learns to divide the post-activation features by the standard deviation part of GroupNorm [4] (GN). Note this is not equivalent to applying GN and Swish sequentially. The full expression for GN-Swish is $\frac{x - \mu_{w,h,c/g}}{\sqrt{s_{w,h,c/g}^2(x)}} \sigma\left(v_1 \frac{x - \mu_{w,h,c/g}}{\sqrt{s_{w,h,c/g}^2(x)}}\right)$ whereas the expression for EvoNorm-S0 is $\frac{x}{\sqrt{s_{w,h,c/g}^2(x)}} \sigma(v_1x)$ (omitting γ and β). The latter is more compact and efficient.

The overall structure of EvoNorm-S0 offers an interesting hint that Swish-like nonlinearities and grouped normalizers may be complementary with each other. Although both GN and Swish have been popular in the literature, their combination is under-explored to the best of our knowledge. In Table 8 we evaluate GN-Swish and compare it with other layers that are batch-independent. The results confirm that both EvoNorm-S0 and GN-Swish can indeed outperform GN-ReLU by a clear margin, though EvoNorm-S0 generalizes better on MobileNetV2.

Scale Invariance. Interestingly, most EvoNorms attempt to promote scale-invariance, an intriguing property from the optimization perspective [65, 66]. See Appendix E.2 for more analysis.

6 Conclusion

In this work, we unify normalization layer and activation function as single tensor-to-tensor computation graph consisting of basic mathematical functions. Unlike mainstream NAS works that specialize a network based on existing layers (Conv-BN-ReLU), we aim to discover new layers that can generalize well across many different architectures. We first identify challenges including high search space sparsity and the weak generalization issue. We then propose techniques to overcome these challenges using efficient rejection protocols and multi-objective evolution. Our method discovered novel layers with surprising structures that achieve strong generalization across many architectures and tasks.

Layer	R-50	MV2
BN-ReLU	70.9 \pm 0.3	66.7 \pm 1.9
GN-ReLU	75.8 \pm 0.1	72.4 \pm 0.1
GN-Swish	76.5 \pm 0.0	73.1 \pm 0.1
EvoNorm-S0	76.5 \pm 0.1	74.0 \pm 0.1

Table 8: ImageNet classification accuracies of ResNet-50 and MobileNetV2 with 4 images/worker.

Acknowledgements

The authors would like to thank Gabriel Bender, Chen Liang, Esteban Real, Sergey Ioffe, Prajit Ramachandran, Pengchong Jin, Xianzhi Du, Ekin D. Cubuk, Barret Zoph, Da Huang, and Mingxing Tan for their comments and support.

References

- [1] Sergey Ioffe and Christian Szegedy. Batch normalization: Accelerating deep network training by reducing internal covariate shift. In *International Conference on Machine Learning*, 2015.
- [2] Jimmy Lei Ba, Jamie Ryan Kiros, and Geoffrey E Hinton. Layer normalization. *arXiv preprint arXiv:1607.06450*, 2016.
- [3] Dmitry Ulyanov, Andrea Vedaldi, and Victor Lempitsky. Instance normalization: The missing ingredient for fast stylization. *arXiv preprint arXiv:1607.08022*, 2016.
- [4] Yuxin Wu and Kaiming He. Group normalization. In *Proceedings of the European Conference on Computer Vision (ECCV)*, pages 3–19, 2018.
- [5] Vinod Nair and Geoffrey E Hinton. Rectified linear units improve restricted boltzmann machines. In *Proceedings of the 27th international conference on machine learning (ICML-10)*, pages 807–814, 2010.
- [6] Andrew L Maas, Awni Y Hannun, and Andrew Y Ng. Rectifier nonlinearities improve neural network acoustic models. In *ICML Workshop on Deep Learning for Audio, Speech, and Language Processing*, 2013.
- [7] Kaiming He, Xiangyu Zhang, Shaoqing Ren, and Jian Sun. Delving deep into rectifiers: Surpassing human-level performance on imagenet classification. In *Proceedings of the IEEE international conference on computer vision*, pages 1026–1034, 2015.
- [8] Djork-Arné Clevert, Thomas Unterthiner, and Sepp Hochreiter. Fast and accurate deep network learning by exponential linear units (elus). *International Conference on Learning Representations*, 2016.
- [9] Dan Hendrycks and Kevin Gimpel. Gaussian error linear units (gelus). *arXiv preprint arXiv:1606.08415*, 2016.
- [10] Günter Klambauer, Thomas Unterthiner, Andreas Mayr, and Sepp Hochreiter. Self-normalizing neural networks. In *Advances in neural information processing systems*, pages 971–980, 2017.
- [11] Prajit Ramachandran, Barret Zoph, and Quoc V Le. Searching for activation functions. In *ICLR Workshop*, 2018.
- [12] Kaiming He, Xiangyu Zhang, Shaoqing Ren, and Jian Sun. Deep residual learning for image recognition. In *Proceedings of the IEEE conference on computer vision and pattern recognition*, pages 770–778, 2016.
- [13] Kaiming He, Xiangyu Zhang, Shaoqing Ren, and Jian Sun. Identity mappings in deep residual networks. In *European conference on computer vision*, pages 630–645. Springer, 2016.
- [14] Mark Sandler, Andrew Howard, Menglong Zhu, Andrey Zhmoginov, and Liang-Chieh Chen. Mobilenetv2: Inverted residuals and linear bottlenecks. In *Proceedings of the IEEE conference on computer vision and pattern recognition*, pages 4510–4520, 2018.
- [15] Mingxing Tan and Quoc V Le. EfficientNet: Rethinking model scaling for convolutional neural networks. In *International Conference on Machine Learning*, 2019.
- [16] Kaiming He, Georgia Gkioxari, Piotr Dollár, and Ross Girshick. Mask r-cnn. In *Proceedings of the IEEE international conference on computer vision*, pages 2961–2969, 2017.
- [17] Tsung-Yi Lin, Piotr Dollár, Ross Girshick, Kaiming He, Bharath Hariharan, and Serge Belongie. Feature pyramid networks for object detection. In *Proceedings of the IEEE conference on computer vision and pattern recognition*, pages 2117–2125, 2017.
- [18] Xianzhi Du, Tsung-Yi Lin, Pengchong Jin, Golnaz Ghiasi, Mingxing Tan, Yin Cui, Quoc V. Le, and Xiaodan Song. Spinenet: Learning scale-permuted backbone for recognition and localization. In *Proceedings of the IEEE Conference on Computer Vision and Pattern Recognition*, 2020.
- [19] Andrew Brock, Jeff Donahue, and Karen Simonyan. Large scale gan training for high fidelity natural image synthesis. In *International Conference on Learning Representations*, 2019.
- [20] Mingxing Tan, Bo Chen, Ruoming Pang, Vijay Vasudevan, Mark Sandler, Andrew Howard, and Quoc V Le. Mnasnet: Platform-aware neural architecture search for mobile. In *Proceedings of the IEEE Conference on Computer Vision and Pattern Recognition*, pages 2820–2828, 2019.
- [21] Xianzhi Du, Tsung-Yi Lin, Pengchong Jin, Golnaz Ghiasi, Mingxing Tan, Yin Cui, Quoc V Le, and Xiaodan Song. Spinenet: Learning scale-permuted backbone for recognition and localization. *arXiv preprint arXiv:1912.05027*, 2019.

- [22] Saurabh Singh and Shankar Krishnan. Filter response normalization layer: Eliminating batch dependence in the training of deep neural networks. *arXiv preprint arXiv:1911.09737*, 2019.
- [23] Ping Luo, Jiamin Ren, Zhanglin Peng, Ruimao Zhang, and Jingyu Li. Differentiable learning-to-normalize via switchable normalization. *International Conference on Learning Representations*, 2019.
- [24] Kenneth O Stanley and Risto Miikkulainen. Efficient reinforcement learning through evolving neural network topologies. In *Proceedings of the 4th Annual Conference on Genetic and Evolutionary Computation*, pages 569–577, 2002.
- [25] Justin Bayer, Daan Wierstra, Julian Togelius, and Jürgen Schmidhuber. Evolving memory cell structures for sequence learning. In *International Conference on Artificial Neural Networks*, pages 755–764. Springer, 2009.
- [26] Barret Zoph and Quoc V Le. Neural architecture search with reinforcement learning. In *International Conference on Learning Representations*, 2017.
- [27] Bowen Baker, Otkrist Gupta, Nikhil Naik, and Ramesh Raskar. Designing neural network architectures using reinforcement learning. In *International Conference on Learning Representations*, 2017.
- [28] Barret Zoph, Vijay Vasudevan, Jonathon Shlens, and Quoc V Le. Learning transferable architectures for scalable image recognition. In *Proceedings of the IEEE conference on computer vision and pattern recognition*, pages 8697–8710, 2018.
- [29] Hanxiao Liu, Karen Simonyan, Oriol Vinyals, Chrisantha Fernando, and Koray Kavukcuoglu. Hierarchical representations for efficient architecture search. In *International Conference on Learning Representations*, 2018.
- [30] Andrew Brock, Theodore Lim, James M Ritchie, and Nick Weston. Smash: one-shot model architecture search through hypernetworks. *arXiv preprint arXiv:1708.05344*, 2017.
- [31] Chenxi Liu, Barret Zoph, Maxim Neumann, Jonathon Shlens, Wei Hua, Li-Jia Li, Li Fei-Fei, Alan Yuille, Jonathan Huang, and Kevin Murphy. Progressive neural architecture search. In *Proceedings of the European Conference on Computer Vision (ECCV)*, pages 19–34, 2018.
- [32] Hanxiao Liu, Karen Simonyan, and Yiming Yang. Darts: Differentiable architecture search. *arXiv preprint arXiv:1806.09055*, 2018.
- [33] Renqian Luo, Fei Tian, Tao Qin, Enhong Chen, and Tie-Yan Liu. Neural architecture optimization. In *Advances in neural information processing systems*, pages 7816–7827, 2018.
- [34] Gabriel Bender, Pieter-Jan Kindermans, Barret Zoph, Vijay Vasudevan, and Quoc Le. Understanding and simplifying one-shot architecture search. In *International Conference on Machine Learning*, pages 550–559, 2018.
- [35] Sirui Xie, Hehui Zheng, Chunxiao Liu, and Liang Lin. Snas: stochastic neural architecture search. *arXiv preprint arXiv:1812.09926*, 2018.
- [36] Han Cai, Ligeng Zhu, and Song Han. Proxylessnas: Direct neural architecture search on target task and hardware. *arXiv preprint arXiv:1812.00332*, 2018.
- [37] Thomas Elsken, Jan Hendrik Metzen, and Frank Hutter. Neural architecture search: A survey. *arXiv preprint arXiv:1808.05377*, 2018.
- [38] Thomas Elsken, Jan Hendrik Metzen, and Frank Hutter. Efficient multi-objective neural architecture search via lamarckian evolution. *arXiv preprint arXiv:1804.09081*, 2018.
- [39] Hieu Pham, Melody Y Guan, Barret Zoph, Quoc V Le, and Jeff Dean. Efficient neural architecture search via parameter sharing. *arXiv preprint arXiv:1802.03268*, 2018.
- [40] Esteban Real, Alok Aggarwal, Yanping Huang, and Quoc V Le. Regularized evolution for image classifier architecture search. In *Proceedings of the AAAI conference on artificial intelligence*, volume 33, pages 4780–4789, 2019.
- [41] Saining Xie, Alexander Kirillov, Ross Girshick, and Kaiming He. Exploring randomly wired neural networks for image recognition. In *Proceedings of the IEEE International Conference on Computer Vision*, pages 1284–1293, 2019.
- [42] Bichen Wu, Xiaoliang Dai, Peizhao Zhang, Yanghan Wang, Fei Sun, Yiming Wu, Yuandong Tian, Peter Vajda, Yangqing Jia, and Kurt Keutzer. Fbnet: Hardware-aware efficient convnet design via differentiable neural architecture search. In *Proceedings of the IEEE Conference on Computer Vision and Pattern Recognition*, pages 10734–10742, 2019.
- [43] Zichao Guo, Xiangyu Zhang, Haoyuan Mu, Wen Heng, Zechun Liu, Yichen Wei, and Jian Sun. Single path one-shot neural architecture search with uniform sampling. *arXiv preprint arXiv:1904.00420*, 2019.
- [44] Hanzhang Hu, John Langford, Rich Caruana, Saurajit Mukherjee, Eric J Horvitz, and Debadepta Dey. Efficient forward architecture search. In *Advances in Neural Information Processing Systems*, pages 10122–10131, 2019.

- [45] Han Cai, Chuang Gan, and Song Han. Once for all: Train one network and specialize it for efficient deployment. *arXiv preprint arXiv:1908.09791*, 2019.
- [46] Liam Li and Ameet Talwalkar. Random search and reproducibility for neural architecture search. *arXiv preprint arXiv:1902.07638*, 2019.
- [47] Xin Chen, Lingxi Xie, Jun Wu, and Qi Tian. Progressive differentiable architecture search: Bridging the depth gap between search and evaluation. In *Proceedings of the IEEE International Conference on Computer Vision*, pages 1294–1303, 2019.
- [48] Dimitrios Stamoulis, Ruizhou Ding, Di Wang, Dimitrios Lymberopoulos, Bodhi Priyantha, Jie Liu, and Diana Marculescu. Single-path nas: Designing hardware-efficient convnets in less than 4 hours. *arXiv preprint arXiv:1904.02877*, 2019.
- [49] Andrew Howard, Mark Sandler, Grace Chu, Liang-Chieh Chen, Bo Chen, Mingxing Tan, Weijun Wang, Yukun Zhu, Ruoming Pang, Vijay Vasudevan, et al. Searching for mobilenetv3. In *Proceedings of the IEEE International Conference on Computer Vision*, pages 1314–1324, 2019.
- [50] Esteban Real, Chen Liang, David R So, and Quoc V Le. Automl-zero: Evolving machine learning algorithms from scratch. *arXiv preprint arXiv:2003.03384*, 2020.
- [51] Hongyi Zhang, Yann N Dauphin, and Tengyu Ma. Fixup initialization: Residual learning without normalization. In *International Conference on Learning Representations*, 2019.
- [52] Soham De and Samuel L Smith. Batch normalization biases deep residual networks towards shallow paths. *arXiv preprint arXiv:2002.10444*, 2020.
- [53] Thomas Bachlechner, Bodhisattwa Prasad Majumder, Huanru Henry Mao, Garrison W Cottrell, and Julian McAuley. Rezero is all you need: Fast convergence at large depth. *arXiv preprint arXiv:2003.04887*, 2020.
- [54] David E Goldberg and Kalyanmoy Deb. A comparative analysis of selection schemes used in genetic algorithms. In *Foundations of genetic algorithms*, volume 1, pages 69–93. Elsevier, 1991.
- [55] A. Krizhevsky and G. Hinton. Learning multiple layers of features from tiny images. *Master’s thesis, Department of Computer Science, University of Toronto*, 2009.
- [56] Kalyanmoy Deb, Amrit Pratap, Sameer Agarwal, and TAMT Meyarivan. A fast and elitist multiobjective genetic algorithm: Nsga-ii. *IEEE transactions on evolutionary computation*, 6(2):182–197, 2002.
- [57] Ekin D Cubuk, Barret Zoph, Jonathon Shlens, and Quoc V Le. Randaugment: Practical data augmentation with no separate search. *arXiv preprint arXiv:1909.13719*, 2019.
- [58] Ilya Loshchilov and Frank Hutter. Sgdr: Stochastic gradient descent with warm restarts. In *International Conference on Learning Representations*, 2017.
- [59] Priya Goyal, Piotr Dollár, Ross Girshick, Pieter Noordhuis, Lukasz Wesolowski, Aapo Kyrola, Andrew Tulloch, Yangqing Jia, and Kaiming He. Accurate, large minibatch sgd: Training imagenet in 1 hour. *arXiv preprint arXiv:1706.02677*, 2017.
- [60] Tsung-Yi Lin, Michael Maire, Serge Belongie, James Hays, Pietro Perona, Deva Ramanan, Piotr Dollár, and C Lawrence Zitnick. Microsoft coco: Common objects in context. In *European conference on computer vision*, pages 740–755. Springer, 2014.
- [61] Ian Goodfellow, Jean Pouget-Abadie, Mehdi Mirza, Bing Xu, David Warde-Farley, Sherjil Ozair, Aaron Courville, and Yoshua Bengio. Generative adversarial nets. In *Advances in neural information processing systems*, pages 2672–2680, 2014.
- [62] Tim Salimans, Ian Goodfellow, Wojciech Zaremba, Vicki Cheung, Alec Radford, and Xi Chen. Improved techniques for training gans. In *Advances in neural information processing systems*, pages 2234–2242, 2016.
- [63] Martin Heusel, Hubert Ramsauer, Thomas Unterthiner, Bernhard Nessler, and Sepp Hochreiter. Gans trained by a two time-scale update rule converge to a local nash equilibrium. In *Advances in neural information processing systems*, pages 6626–6637, 2017.
- [64] Tero Karras, Timo Aila, Samuli Laine, and Jaakko Lehtinen. Progressive growing of gans for improved quality, stability, and variation. In *International Conference on Learning Representations*, 2018.
- [65] Elad Hoffer, Ron Banner, Itay Golan, and Daniel Soudry. Norm matters: efficient and accurate normalization schemes in deep networks. In *Advances in Neural Information Processing Systems*, pages 2160–2170, 2018.
- [66] Zhiyuan Li and Sanjeev Arora. An exponential learning rate schedule for deep learning. In *International Conference on Learning Representations*, 2020.

A Code Snippets in TensorFlow

The following pseudocode relies on broadcasting to make sure the tensor shapes are compatible.

BN-ReLU

```
def batchnorm_relu(x, gamma, beta, nonlinearity, training):
    mean, std = batch_mean_and_std(x, training)
    z = (x - mean) / std * gamma + beta
    if nonlinearity:
        return tf.nn.relu(z)
    else:
        return z
```

EvoNorm-B0 (use this to replace BN-ReLU)

```
def evonorm_b0(x, gamma, beta, nonlinearity, training):
    if nonlinearity:
        v = trainable_variable_ones(shape=gamma.shape)
        _, batch_std = batch_mean_and_std(x, training)
        den = tf.maximum(batch_std, v * x + instance_std(x))
        return x / den * gamma + beta
    else:
        return x * gamma + beta
```

EvoNorm-S0 (use this to replace BN-ReLU)

```
def evonorm_s0(x, gamma, beta, nonlinearity):
    if nonlinearity:
        v = trainable_variable_ones(shape=gamma.shape)
        num = x * tf.nn.sigmoid(v * x)
        return num / group_std(x) * gamma + beta
    else:
        return x * gamma + beta
```

Helper functions for EvoNorms

```
def instance_std(x, eps=1e-5):
    _, var = tf.nn.moments(x, axes=[1, 2], keepdims=True)
    return tf.sqrt(var + eps)

def group_std(x, groups=32, eps=1e-5):
    N, H, W, C = x.shape
    x = tf.reshape(x, [N, H, W, groups, C // groups])
    _, var = tf.nn.moments(x, [1, 2, 4], keepdims=True)
    std = tf.sqrt(var + eps)
    std = tf.broadcast_to(std, x.shape)
    return tf.reshape(std, [N, H, W, C])

def trainable_variable_ones(shape, name="v"):
    return tf.get_variable(name, shape=shape,
                           initializer=tf.ones_initializer())
```

B Proxy Task and Anchor Architectures

An ideal proxy task should be lightweight enough to allow speedy feedback. At the same time, the anchor architectures must be sufficiently challenging to train from the optimization point of view to stress-test the layers. These motivated us to consider a small training task and deep architectures.

We therefore define the proxy task as image classification on the CIFAR-10 dataset [55], and consider three representative ImageNet architectures (that are deep enough) adapted with respect to this setup, including Pre-activation ResNet50 [13] with channel multiplier $0.25\times$, MobileNetV2 [14] with channel multiplier $0.5\times$ and EfficientNet-B0 [15] with channel multiplier $0.5\times$. To handle the reduced image resolution on CIFAR-10 relative to ImageNet, the first two convolutions with spatial reduction are modified to use stride one for all of these architectures. We refer to these adapted versions as ResNet50-CIFAR, MobileNetV2-CIFAR and EfficientNet-CIFAR, respectively. We do not change anything beyond channel multipliers and strides described above, to preserve the original attributes (e.g., depth) of these ImageNet models as much as possible.

C Implementation Details

Proxy Task on CIFAR-10. We use the same training setup for all the architectures. Specifically, we use 24×24 random crops on CIFAR-10 with a batch size of 128 for training, and use the original 32×32 image with a batch size of 512 for validation. We use SGD with learning rate 0.1, Nesterov momentum 0.9 and weight decay 10^{-4} . Each model is trained for 2000 steps with a constant learning rate for the EvoNorm-B experiment. Each model is trained for 5000 steps following a cosine learning rate schedule for the EvoNorm-S experiment. These are chosen to ensure the majority of the models can achieve reasonable convergence quickly. With our implementation, it takes 3-10 hours to train each model on a single CPU worker with two cores.

Evolution. We regularize the evolution [40] by considering a sliding window of only the most recent 2500 genotypes. Each tournament is formed by a random subset of 5% of the active population. Winner is determined as a random candidate on the Pareto-frontier w.r.t. the three accuracy scores (Sec. 4.1), which will be mutated twice in order to promote structural diversity. To encourage exploration, we further inject noise into the evolution process by replacing the offspring with a completely new random architecture with probability 0.5. Each search experiment takes 2 days to complete with 5000 CPU workers.

Reranking. After search, we take the top-10 candidates from evolution and pair each of them with fully-fledged ResNet-50, MobileNetV2 and EfficientNet-B0. We then rerank the layers based on their averaged ImageNet accuracies of the three models. To avoid overfitting the validation/test metric, each model is trained using 90% of the ImageNet *training* set and evaluated over the rest of the 10%. The top-3 reranked layers are then used to obtain our main results. The reranking task is more computationally expensive than the proxy task we search with, but is accordingly more representative of the downstream tasks of interest, allowing for better distinguishing between top candidates.

Classification on ImageNet. For ImageNet results presented in Table 3 (layers with batch statistics), we use a base learning rate of 0.1 per 256 images for ResNets, MobileNetV2 and MnasNet, and a base learning rate of 0.016 per 256 images for EfficientNets following the official implementation. Note these learning rates have been heavily optimized w.r.t. batch normalization. For results presented in Table 4 (layers without batch statistics), the base learning rate for MobileNetV2 is lowered to 0.03 (tuned w.r.t. GN-ReLU among 0.01, 0.03, 0.1). We use the standard multi-stage learning rate schedule in the basic training setting for ResNets, cosine schedule [58] for MobileNetV2 and MnasNet, and the original polynomial schedule for EfficientNets. These learning rate schedules also come with a linear warmup phase [59]. For all architectures, the batch size per worker is 128 and the input resolution is 224×224 . The only exception is EfficientNet-B5, which uses batch size 64 per worker and input resolution 456×456 . The number of workers is 8 for ResNets and 32 for the others. We use 32 groups for grouped aggregation ops $\mu_{w,h,c/g}$ and $s_{w,h,c/g}^2$.

Instance Segmentation on COCO The training is carried out over 8 workers with 8 images/worker and the image resolution is 1024×1024 . The models are trained from scratch for 135K steps using SGD with momentum 0.9, weight decay $4e-5$ and an initial learning rate of 0.1, which is reduced by $10 \times$ at step 120K and step 125K. For SpineNet experiments, we follow the training setup of the original paper [21].

D Candidate layers without Reranking

D.1 Top-10 EvoNorm-B candidates

1. $\frac{x}{\max(\sqrt{s_{b,w,h}^2(x,z)})} \gamma + \beta, z = (x + 1) \sqrt{\mu_{w,h}(x^2)}$
2. $\frac{x}{\max(\sqrt{s_{b,w,h}^2(x,z)})} \gamma + \beta, z = x + \sqrt{\mu_{w,h,c}(x^2)}$
3. $-\frac{x\sigma(x)}{\sqrt{s_{b,w,h}^2(x)}} \gamma + \beta$
4. $\frac{x}{\max(\sqrt{s_{b,w,h}^2(x,z)})} \gamma + \beta, z = x \sqrt{\mu_{w,h}(x^2)}$

5. $\frac{x}{\max(\sqrt{s_{b,w,h}^2(x)}, z)}\gamma + \beta, z = \sqrt{\mu_{w,h,c}(x^2)} - x$
6. $\frac{x}{\max(\sqrt{s_{b,w,h}^2(x)}, z)}\gamma + \beta, v_1x + \sqrt{s_{w,h}^2(x)}$
7. $\frac{x}{\max(\sqrt{s_{b,w,h}^2(x)}, z)}\gamma + \beta, z = \sqrt{\mu_{w,h}(x^2)} - x$
8. $\frac{x}{\max(\sqrt{s_{b,w,h}^2(x)}, z)}\gamma + \beta, z = x\sqrt{\mu_{w,h}(x^2)}$ (duplicate)
9. $\frac{x}{\max(\sqrt{s_{b,w,h}^2(x)}, z)}\gamma + \beta, z = x + \sqrt{s_{w,h}^2(x)}$
10. $\frac{x}{\max(\sqrt{s_{b,w,h}^2(x)}, z)}\gamma + \beta, z = x + \sqrt{s_{w,h}^2(x)}$ (duplicate)

D.2 Top-10 EvoNorm-S candidates

1. $\frac{x \tanh(\sigma(x))}{\sqrt{\mu_{w,h,c/g}(x^2)}}\gamma + \beta$
2. $\frac{x\sigma(x)}{\sqrt{\mu_{w,h,c/g}(x^2)}}\gamma + \beta$
3. $\frac{x\sigma(x)}{\sqrt{\mu_{w,h,c/g}(x^2)}}\gamma + \beta$ (duplicate)
4. $\frac{x\sigma(x)}{\sqrt{\mu_{w,h,c/g}(x^2)}}\gamma + \beta$ (duplicate)
5. $\frac{x\sigma(x)}{\sqrt{s_{w,h,c/g}^2(x)}}\gamma + \beta$
6. $\frac{x\sigma(v_1x)}{\sqrt{s_{w,h,c/g}^2(x)}}\gamma + \beta$
7. $\frac{x\sigma(x)}{\sqrt{s_{w,h,c/g}^2(x)}}\gamma + \beta$ (duplicate)
8. $\frac{x\sigma(x)}{\sqrt{\mu_{w,h,c/g}(x^2)}}\gamma + \beta$ (duplicate)
9. $\frac{x\sigma(x)}{\sqrt{s_{w,h,c/g}^2(x)}}\gamma + \beta$ (duplicate)
10. $z\sigma(\max(x, z))\gamma + \beta, z = \frac{x}{\sqrt{\mu_{w,h,c/g}(x^2)}}$

E Additional Results

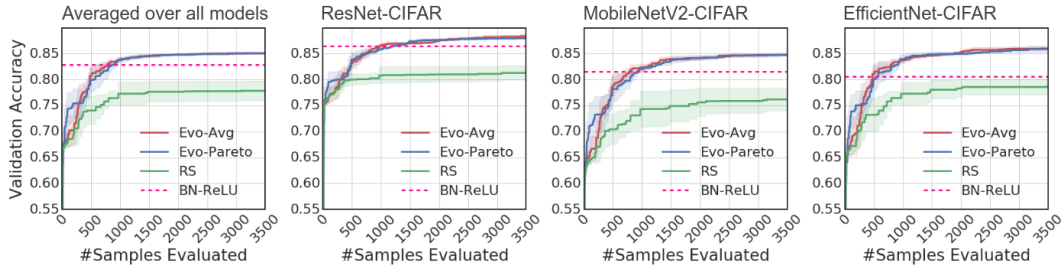


Figure 7: Search progress of evolution vs. random search vs. a fixed baseline (BN-ReLU) on the proxy task. Each curve denotes the mean and standard deviation of the top-10 architectures in the population. Only valid samples survived the rejection phase are reported.

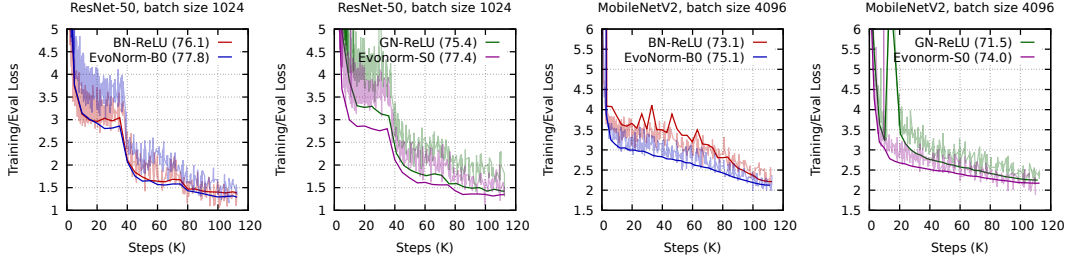


Figure 8: Training/eval curves for ResNet-50 (+aug) and MobileNetV2 on ImageNet with large batch sizes. The corresponding test accuracy for each layer is reported in the legend.

Layer	Images / Worker					
	128	64	32	16	8	4
BN-ReLU	76.1	76.4	76.3	76.0	74.5	70.4
GN-ReLU	75.1	75.8	75.9	75.8	75.7	75.8
FRN	75.5	75.8	75.9	75.8	75.8	75.8
EvoNorm-S0	76.2	76.2	76.3	76.3	76.1	76.4
EvoNorm-S1	76.3	76.1	76.2	76.2	76.1	76.4
EvoNorm-S2	76.1	76.3	76.4	76.3	76.3	76.4

Table 9: ResNet-50 results as the batch size decreases (90 training epochs, original learning rate schedule).

Layer	Images / Worker					
	128	64	32	16	8	4
BN-ReLU	77.6	77.6	77.1	76.7	74.8	72.0
GN-ReLU	76.9	77.1	77.0	77.0	77.0	77.2
FRN	77.2	77.1	77.2	77.1	76.8	77.2
EvoNorm-S0	78.0	77.8	77.9	78.1	78.1	77.8
EvoNorm-S1	77.9	77.8	78.0	77.8	77.8	78.0
EvoNorm-S2	77.5	77.7	77.7	77.6	77.6	77.6

Table 11: ResNet-50 results as the batch size decreases (180 training epochs with RandAugment, original learning rate schedule).

Layer	Images / Worker					
	128	64	32	16	8	4
BN-ReLU	73.3	73.2	72.7	70.0	64.5	60.4
GN-ReLU	71.5	72.6	72.9	72.5	72.7	72.6
FRN	73.3	73.4	73.5	73.6	73.5	73.5
EvoNorm-S0	74.0	74.0	73.9	73.9	73.9	73.8
EvoNorm-S1	73.7	74.0	73.6	73.7	73.7	73.8
EvoNorm-S2	73.8	73.4	73.7	73.9	73.9	73.8

Table 13: MobileNetV2 results as the batch size decreases.

Layer	Images / Worker					
	128	64	32	16	8	4
BN-ReLU	76.1	76.2	76.1	75.6	74.3	70.7
GN-ReLU	75.4	75.7	75.9	75.8	75.8	75.7
FRN	75.3	75.8	75.9	75.9	75.8	76.0
EvoNorm-S0	77.4	77.4	77.6	77.3	77.3	77.5
EvoNorm-S1	77.5	77.3	77.4	77.4	77.3	77.4
EvoNorm-S2	76.9	77.3	77.1	77.2	77.1	77.1

Table 10: ResNet-50 results as the batch size decreases (90 training epochs with RandAugment, original learning rate schedule).

Layer	Images / Worker					
	128	64	32	16	8	4
BN-ReLU	77.7	77.6	77.2	76.3	74.5	70.6
GN-ReLU	77.1	77.2	77.3	77.3	77.3	77.3
FRN	77.2	77.4	77.4	77.2	77.4	77.4
EvoNorm-S0	78.3	78.3	78.4	78.3	78.2	78.2
EvoNorm-S1	78.2	78.2	78.3	78.1	78.1	78.2
EvoNorm-S2	78.2	78.1	78.0	77.9	77.9	78.0

Table 12: ResNet-50 results as the batch size decreases (180 training epochs with RandAugment, cosine learning rate schedule).



Figure 9: Selected samples from BigGAN-deep + EvoNorm-B0.

E.1 Trade-off on Lightweight Models

Batch normalization is efficient thanks to its simplicity and the fact that both the moving averages and affine parameters can be fused into adjacent convolutions during inference. EvoNorms, despite being more powerful, can come with more sophisticated expressions. While the overhead is negligible even for medium-sized models (Table 5), it can be nontrivial for lightweight, mobile-sized models.

We study this subject in detail using MobileNetV2 as an example, showing that EvoNorm-B0 in fact substantially outperforms BN-ReLU in terms of both accuracy-parameters trade-off and

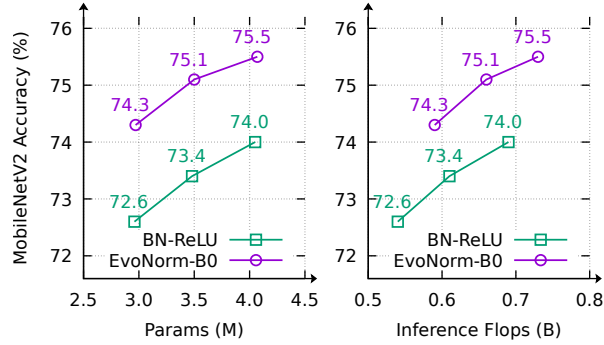


Figure 10: ImageNet accuracy vs. params and accuracy vs. FLOPs for MobileNetV2 paired with different normalization-activation layers. Each layer is evaluated over three model variants with channel multipliers $0.9\times$, $1.0\times$ and $1.1\times$. We consider the inference-mode FLOPs for both BN-ReLU and EvoNorm-B0, allowing parameter fusion with adjacency convolutions whenever possible.

accuracy-FLOPs trade-off (Figure 10). This is because the cost overhead of EvoNorms can be largely compensated by their performance gains.

E.2 Scale-invariance of EvoNorms

It is intriguing to see that EvoNorm-B0 keeps the scale invariance property of traditional layers, which means rescaling the input x would not affect its output. EvoNorm-S0 is asymptotically scale-invariant in the sense that it will reduce to either $\frac{x}{\sqrt{s_{w,h,c/g}^2}}$ or a constant zero when the magnitude of x becomes large, depending on the sign of v_1 . The same pattern is also observed for most of the EvoNorm candidates presented in Appendix D. These observations are aligned with previous findings that scale invariance might play a useful role in optimization [65, 66].